Am J Physiol Heart Circ Physiol 315: H699–H708, 2018.
First published June 8, 2018; doi:10.1152/ajpheart.00047.2018.

RESEARCH ARTICLE | *Right Ventricular Physiology in Health and Disease*

Multiscale structure-function relationships in right ventricular failure due to pressure overload

Tik-Chee Cheng,[1]* Jennifer L. Philip,[1,2]* Diana M. Tabima,[1] Timothy A. Hacker,[3] and Naomi C. Chesler[1,3]

[1]*Department of Biomedical Engineering, University of Wisconsin-Madison College of Engineering, Madison, Wisconsin;* [2]*Department of Surgery, University of Wisconsin-Madison, Madison, Wisconsin; and* [3]*Department of Medicine, University of Wisconsin-Madison, Madison, Wisconsin*

Submitted 19 January 2018; accepted in final form 6 June 2018

Cheng TC, Philip JL, Tabima DM, Hacker TA, Chesler NC. Multiscale structure-function relationships in right ventricular failure due to pressure overload. *Am J Physiol Heart Circ Physiol* 315: H699–H708, 2018. First published June 8, 2018; doi:10.1152/ajpheart.00047.2018.—Right ventricular (RV) failure (RVF) is the major cause of death in pulmonary hypertension. Recent studies have characterized changes in RV structure in RVF, including hypertrophy, fibrosis, and abnormalities in mitochondria. Few, if any, studies have explored the relationships between these multiscale structural changes and functional changes in RVF. Pulmonary artery banding (PAB) was used to induce RVF due to pressure overload in male rats. Eight weeks postsurgery, terminal invasive measurements demonstrated RVF with decreased ejection fraction (70 ± 10 vs. 45 ± 15%, sham vs. PAB, $P < 0.005$) and cardiac output (126 ± 40 vs. 67 ± 32 ml/min, sham vs. PAB, $P < 0.05$). At the organ level, RV hypertrophy was directly correlated with increased contractility, which was insufficient to maintain ventricular-vascular coupling. At the tissue level, there was a 90% increase in fibrosis that had a direct correlation with diastolic dysfunction measured by reduced chamber compliance ($r^2 = 0.43$, $P = 0.008$). At the organelle level, transmission electron microscopy demonstrated an abundance of small-sized mitochondria. Increased mitochondria was associated with increased ventricular oxygen consumption and reduced mechanical efficiency ($P < 0.05$). These results demonstrate an association between alterations in mitochondria and RV oxygen consumption and mechanical inefficiency in RVF and a link between fibrosis and in vivo diastolic dysfunction. Overall, this work provides key insights into multiscale RV remodeling in RVF due to pressure overload.

NEW & NOTEWORTHY This study explores the functional impact of multiscale ventricular remodeling in right ventricular failure (RVF). It demonstrates correlations between hypertrophy and increased contractility as well as fibrosis and diastolic function. This work quantifies mitochondrial ultrastructural remodeling in RVF and demonstrates increased oxygen consumption and mechanical inefficiency as features of RVF. Direct correlation between mitochondrial changes and ventricular energetics provides insight into the impact of organelle remodeling on organ level function.

right ventricular failure; pressure-volume loops; pulmonary artery banding; mitochondria; myocardial energetics

INTRODUCTION

Right ventricular (RV) failure (RVF) is the primary cause of death in patients suffering from pulmonary arterial hypertension (PAH), which is a debilitating disease with a prevalence of 6.6−26 per 1 million adults (1, 18) characterized by a progressive increase in RV afterload (10, 48). RVF is defined as the inability to maintain RV cardiac output (CO) and ejection fraction (EF) despite normal preload (17, 29). Recent studies have begun to characterize the multiscale structural remodeling occurring in the RV in response to pressure overload, but the impact of these structural changes on ventricular function remains largely unknown. Understanding structure-function relationships has the potential to provide important insight into disease mechanisms and development of effective therapies for RVF.

At the organ level, the initial response to increased afterload is ventricular hypertrophy (7, 49). RVF is thought to occur when this adaptive remodeling is insufficient to compensate for the persistent increase in RV afterload (7, 8, 49). The functional impact of hypertrophy is accepted to be an increase in contractility, a common feature of patients with PAH (42) and animal models of pressure overload (26, 52). However, the degree to which hypertrophy accounts for functional changes and the relationship between the two has not been fully explored.

At the tissue level, RV fibrosis is a histological hallmark of RVF shown to occur in both human disease (35) and small animal models of PAH (2, 11, 34). Recent studies have shown that fibrosis contributes to stiffness of isolated trabeculae (34). However, the impact of fibrosis on RV diastolic function in vivo has not been explored.

At the organelle level, mitochondria are the powerhouse of the heart, and mitochondrial abnormalities play a pivotal role in the development of heart failure (5). Mitochondrial structural and functional abnormalities and altered mitochondrial biogenesis have been identified in animal models of PAH (15, 31). However, despite a growing focus on metabolic remodeling in RVF, it is largely unknown whether mitochondrial structural changes correlate with changes in RV function, particularly oxygen consumption as measured by pressure-volume area (PVA) from pressure-volume loops and mechanical efficiency determined by the ratio of external work (EW) to PVA.

* T. -C. Cheng and J. L. Philip contributed equally to this work.

Address for reprint requests and other correspondence: N. C. Chesler, Univ. of Wisconsin at Madison, 2146 Engineering Centers Bldg., 1550 Engineering Dr., Madison, WI 53706 (e-mail: naomi.chesler@wisc.edu).

The goal of the present study was to examine structure-function relationships across multiple scales in the setting of RVF due to pressure overload. To do so, we created RVF in rats using pulmonary artery banding (PAB). Hemodynamic function of the RV was determined using echocardiography and right heart catheterization. Morphological changes at the organ, tissue, and organelle levels were determined via echocardiography, histology, and transmission electron microscopy, respectively. We found significant correlations between ventricular hypertrophy and increased contractility, ventricular fibrosis and diastolic dysfunction, and mitochondrial remodeling and RV oxygen consumption as well as mechanical inefficiency.

METHODS

Animal model and study design. Adult male Wistar rats ($n = 20$, 230–290 g, Charles River Laboratories, Wilmington, MA) were randomized into two groups: sham ($n = 8$) or PAB ($n = 12$). All rats underwent baseline echocardiography, during which pulmonary artery diameter was measured. After echocardiography, rats underwent PAB or sham surgery. Rats were maintained until 8 wk postsurgery, when they underwent terminal hemodynamic evaluation. All procedures were approved by the University of Wisconsin-Madison Institutional Animal Care and Use Committee.

Echocardiography. Rats were anesthetized with isoflurane (5% and then maintained at 1–2%, balance oxygen). Baseline measurements of pulmonary artery diameter were obtained at end diastole in B-mode images using the Vevo 770 ultrasonograph (VisualSonics, Toronto, ON, Canada). Two-dimensional M-mode images acquired at the papillary muscle were used to measure RV wall thickness and RV inner diameter at end diastole. Heart rate was measured in all rats. All parameters were measured over at least three consecutive cardiac cycles and averaged. Echocardiography was repeated at 2, 4, and 8 wk postsurgery to monitor RV morphological changes in response to PAB.

PAB and sham surgery. Rats were anesthetized with isoflurane (5% and then maintenance at 2–3%, balance oxygen), intubated, and ventilated. After lateral thoracotomy and dissection of the main PA, a silk suture was placed around the main PA. In PAB rats, the suture was tightened around a needle to achieve ~60% constriction by diameter based on the baseline echocardiographic measurement and tied. In sham rats, the suture was neither tightened nor tied. Survival for both PAB and sham surgeries was 100%. Rats were followed for ≤8 wk postoperatively. One PAB rat died 1 wk postsurgery; one PAB rat died 5 wk postsurgery. Neither tissue nor hemodynamic data were collected from these two animals. At the terminal right heart catheterization procedure, PV waveforms were not recorded for an additional two PAB rats and one sham rat due to deterioration in cardiac function after the RV was exposed and interference with catheter placement. Tissue from these three rats was harvested and included in the RV hypertrophy calculation, histology, and biochemical assays.

Hemodynamic measurements of RV and pulmonary vascular function. At 8 wk postsurgery, after rats recovered from echocardiography procedures, invasive right heart catheterization was performed. RV pressure and volume were measured simultaneously, as previously described (47). Briefly, rats were anesthetized with urethane (1.2 g/kg) to maintain heart rate, intubated, and ventilated with room air at a tidal volume of 2–2.5 ml and a respiratory rate of 80–100 breaths/min (41). Subsequently, rats were placed supine on a heated pad to keep the body temperature at ~37°C. The right carotid artery was isolated for systemic pressure monitoring at the aortic arch using a pressure catheter (Millar, Houston, TX). After the chest plate was removed, the pericardium was carefully removed, and a 1.9-Fr variable segment admittance pressure-volume catheter (Scisense, London, ON, Canada) was inserted into the RV through the apex using a 24-gauge needle. All measurements were taken under open-chest conditions. Commercial software (Notocord Systems, Croissy Sur Seine, France) was used to record RV pressure-volume waveforms at 1,000 Hz. After baseline recordings, brief vena cava occlusions were performed to obtain end-systolic pressure-volume relationships.

Hemodynamic calculations. RV function was quantified using well-established parameters derived from RV pressure-volume waveforms, including RV end-systolic pressure, end-diastolic pressure, stroke volume, CO, EF, isovolumic relaxation time constant (τ Weiss), effective arterial elastance (E_a), RV maximal and minimal derivatives of pressure (dP/dt_{max} and dP/dt_{min}), slope of the dP/dt_{max}-end-diastolic volume relationship, and chamber compliance (stroke volume/RV pulse pressure, where pulse pressure was calculated as end-systolic pressure − end-diastolic pressure) (23, 25, 40). To account for weight changes, the cardiac index was calculated as cardiac output normalized to body weight. The load-independent index of systolic function end-systolic elastance (E_{es}) was derived from pressure-volume loops during vena cava occlusions. Ventricular-vascular coupling was quantified as E_{es}/E_a (39, 45, 47). RV energetics and mechanical efficiency were assessed via EW, PVA, and EW/PVA, which were derived from the RV pressure-volume relations (14, 32).

Tissue harvesting and fixation. After hemodynamic measurements, rats were euthanized by exsanguination. Once the heart was excised, the RV free wall was separated from the LV and septum, rinsed in saline, dried, and weighed for the calculation of RV hypertrophy indexes. The RV was segmented and divided for different biochemical assessments. One RV section was immersion fixed in 10% formalin followed by 70% ethanol for histology (50). Another section of the RV was immersed in RNAlater (Thermo Scientific, Rockford, IL) and flash frozen for quantitative real-time PCR analysis. In only five sham and five PAB rats, a third RV segment of 2–3 mm long and ~1 mm thick was immersion fixed in ice-cold Karnovsky's fixative at 4°C for electron microscopy (22).

Histology. RV tissues preserved in ethanol for histology were paraffin embedded and sectioned. As previously reported by our group (14, 50), slides were stained with picrosirius red to identify collagen. An inverted microscope (TE-2000-5, Nikon, Melville, NY) was used to acquire all images using a Spot chargr-coupled device camera (Optical Analysis Systems, Nashua, NH). The area containing collagen was determined by color thresholding in a representative field of view using software (MetaVue, Optical Analysis Systems). Five representative fields of view were taken for each RV. The collagen area was divided by the tissue area in each field of view to calculate the percent collagen area and averaged.

Electron microscopy. After 3 days in Karnovsky's fixative (Electron Microscopy Sciences, Hatfield, PA) composed of 5% glutaraldehyde and 4% paraformaldehyde [0.1 M sodium phosphate buffer (PB), pH 7.2] at 4°C, RV tissue samples were rinsed in PB and postfixed with 0.1% osmium tetroxide, 1% potassium ferrocyanide (in 0.1M PB, pH 7.2) for 60 min, washed with PB, dehydrated in a graded series of ethanol, and infiltrated/flat embedded in a Polybed812 resin (Electron Microscopy Sciences) as previously described (22). Ultrathin sections (90 nm) were collected on a Reichert-Jung Ultracut E ultramicrotome, collected on Pioloform (Ted Pella, Redding, CA)-coated 2 × 1 slot Cu grids, and poststained in uranyl acetate and lead citrate. Samples were examined using a Philips CM120 transmission electron microscope at 80 kV and documented with an Advanced Microscopy Techniques BioSprint12 digital camera.

To quantify mitochondrial number and size and estimate mass, cardiomyocytes were photographed in the longitudinal orientation at ×5,600 magnification. Regions containing visible M-lines and mitochondria were selected for analysis. Individual mitochondria in the transmission electron microscopy images were delineated by manually tracing closed contours around their clearly discernible outer membrane (33). For each rat, at least three micrographs were captured from the single RV tissue section and analyzed using ImageJ

(version 1.49v, National Institutes of Health, Bethesda, MD). Mitochondria per high-power field (HPF) are reported as the average numbers of mitochondria counted in three micrographs (22.5 × 19.4 μm). Mitochondrial size is reported as average cross-sectional area of mitochondria in 3 micrographs/animal in square micrometers. Mitochondrial mass was estimated from the volume fraction of mitochondria (mitochondria/HPF × cross-sectional area/mitochondria ÷ the area of HPF) times RV free wall mass.

Quantitative real-time PCR. With the Qiagen RNeasy Fibrous Tissue kit (Qiagen Sciences, Germantown, MD), mRNA was carefully isolated from 10 mg of homogenized RV tissue according to the manufacturer's protocol. RNA quality (absorbance at 260/280 nm: 1.7 – 2.1) and concentration were measured using a spectrophotometer (Nanodrop 2000). RNA (2 μg) was reverse transcribed into cDNA using a High Capacity cDNA Reverse Transcription Kit (Applied Biosystems, Foster City, CA). Real-time PCR was performed using TaqMan Gene Expression Master Mix according to the manufacturer's instructions (Invitrogen Life Technologies, Carlsbad, CA) and as previously described (16). TaqMan assay primers included the following: peroxisome proliferator-activated receptor (PPAR)-γ coactivator-1α (PGC-1α; ppargc1, Mm01208835_m1) and hypoxanthine phosphoribosyltransferase 1(Hprt1; Rn01527840_m1). Based on the standard curves for the TaqMan gene primers, 4 ng cDNA was used in the PCR for PGC-1α. All PCRs were performed using the Applied Biosystems StepOne Plus Real-Time PCR System. Cycling parameters were as follows: 50°C for 2 min, 95°C for 10 min, and 95°C for 15 s followed by 60°C for 1 min for 40 cycles. Changes in mRNA expression were determined by the comparative threshold cycle ($\Delta\Delta C_T$) method (28). Data were normalized to Hprt1 and expressed as fold change compared with the sham group.

Statistical analysis. All values are presented as means ± SD. A two-tailed Student's *t*-test was used to compare PAB with sham rats for all single end-point measurements. Changes in RV morphology over time from echocardiography were analyzed using repeated-measures ANOVA (baseline vs. 2, 4, and 8 wk postsurgery) with Bonferroni post hoc correction for multiple comparisons. Bivariate correlations were performed using Pearson's correlation analysis. All statistical analyses were performed using IBM SPSS Statistics version 22. *P* values of <0.05 were considered statistically significant.

RESULTS

Signs and symptoms of decompensated RVF due to PAB. The PAB rat that died 5 wk postsurgery exhibited ascites, ruffled fur, low activity, and dyspnea, which are signs and symptoms of decompensated RVF (3, 4). The remaining PAB rats did not show signs or symptoms of decompensated RVF.

PAB resulted in the development of compensated RVF by 8 wk postbanding. PAB resulted in significant pressure overload that was sustained at 8 wk postbanding, with a nearly twofold increase in RV end-systolic pressure (Fig. 1*A*). This pressure overload resulted in compensated RVF, as evidenced by significant reduction in RV EF (Fig. 1*B*) as well as impaired CO (Fig. 1*C*) without the symptoms noted above.

RV hypertrophy associated with increased contractility is insufficient to maintain ventricular-vascular coupling after PAB. Echocardiographic measurements demonstrated significant RV free wall thickening in PAB rats as early as 2 wk postbanding, which was sustained up to 8 wk postbanding (Table 1). Examination of RV tissue at 8 wk postbanding showed a 148% increase in RV weight compared with sham rats (Table 2). Beyond absolute RV weight, RV weight indexed

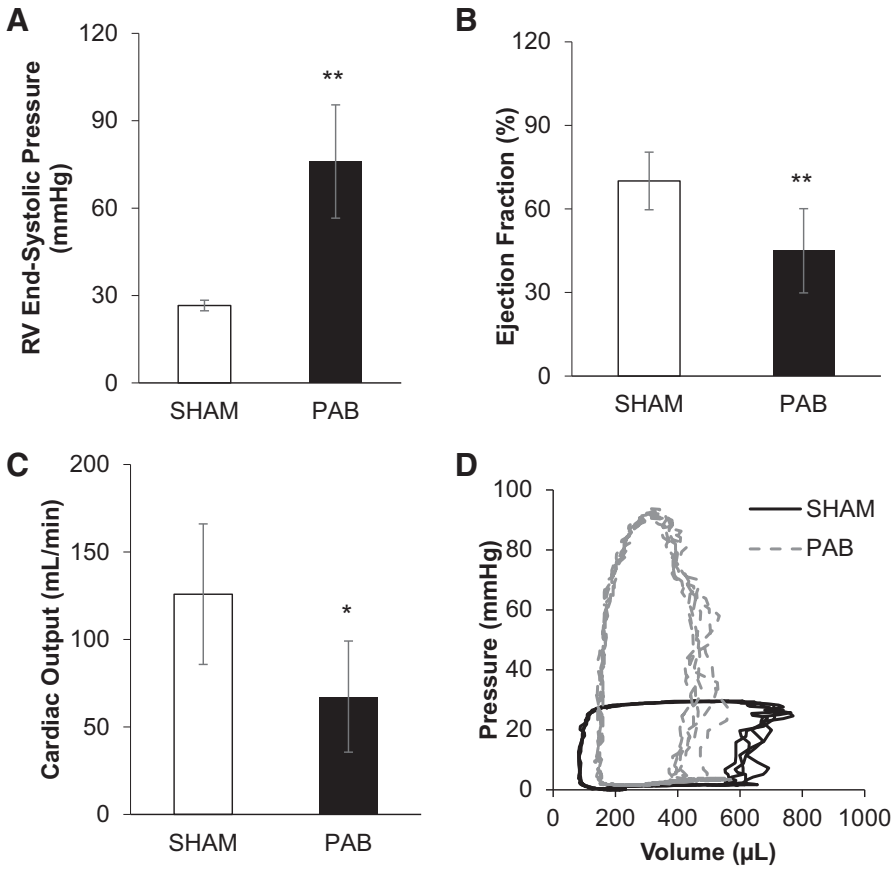

Fig. 1. *A–C*: pulmonary artery banded (PAB) rats exhibited elevated right ventricular (RV) end-systolic pressure (*A*), diminished ejection fraction (*B*), and decreased cardiac output (*C*) compared with sham rats. *D*: representative RV pressure-volume loops measured in sham and PAB rats. Data are presented as means ± SD. A two-tailed Student's *t*-test was used to determine significant differences between groups. $n = 7$ sham and 8 PAB rats. $^*P < 0.05$ and $^{**}P < 0.005$, sham vs. PAB.

Table 1. *Morphological parameters measured using echocardiography*

	Presurgery	*Week 2*	*Week 4*	*Week 8*
Heart rate, beats/min				
Sham	401.8 ± 41.5	399.6 ± 30.1	388.8 ± 28.0	381.1 ± 30.0
PAB	413.2 ± 26.1	347.0 ± 42.4*‡	330.3 ± 38.9†§	341.6 ± 43.6§
RV wall thickness during diastole, mm				
Sham	0.44 ± 0.03	0.51 ± 0.09	0.58 ± 0.07‡	0.52 ± 0.15
PAB	0.43 ± 0.08	0.65 ± 0.10*§	0.71 ± 0.13*§	0.76 ± 0.17*§
RV inner diameter during diastole, mm				
Sham	2.75 ± 0.53	3.06 ± 0.29	3.30 ± 0.59	3.06 ± 0.61
PAB	3.26 ± 0.51	3.51 ± 0.51	4.01 ± 0.78	3.70 ± 0.37*

Values are means ± SD; $n = 8$ sham and 10 pulmonary artery banded (PAB) rats across all time points. RV, right ventricle. Data were recorded before (presurgery) and 2, 4, and 8 wk after surgery for sham and PAB rats. Repeated-measures ANOVA with Bonferroni post hoc correction was used to determine significant differences between groups: *$P < 0.05$ and †$P < 0.005$, sham vs. PAB; ‡$P < 0.05$ and §$P < 0.005$, time point vs. presurgery within group.

to body weight or left ventricular (LV) and septal weight was also significantly higher in the PAB group. There was also an increase in RV contractility after banding, as evidenced by increased E_{es} (Fig. 2*A*), dP/dt_{max} (Fig. 2*D*), and the dP/dt_{max}-end-diastolic volume relationship (Table 3), which was strongly and directly correlated with RV hypertrophy, as assessed by indexed RV mass and RV wall thickness (Fig. 2, *E* and *F*).

Despite these adaptive changes contributing to increased contractilty, RV-pulmonary vascular coupling, as measured by E_{es}/E_a, was not maintained (Fig. 2*C*). That is, the significant 60% increase in E_{es} was insufficient to match the 350% increase in afterload measured by E_a (Fig. 2*B*). Consistent with this finding, there was a trend toward increase in mean RV internal diameter measured during diastole in the PAB group that was significant at the eighth wk (Table 1). RV end-diastolic pressure and end-diastolic volume (Table 3) also showed trends of increase but did not reach statistical significance. These results indicate that PAB animals did not transition from RV hypertrophy to RV dilation.

Ventricular fibrosis is associated with diastolic dysfunction. RV fibrosis was assessed using picrosirus red staining to specifically examine perimyocyte collagen deposition. Qualitative and quantitative analyses demonstrated a dramatic increase in collagen deposition in the PAB group (Fig. 3, *A* and *B*). In addition, RV diastolic function was impaired in vivo after PAB, as evidenced by a significantly increased τ Weiss (Fig. 3*C*), suggesting delayed active relaxation, and significantly reduced chamber compliance (Fig. 3*D*), suggesting passive RV stiffening. We examined the relationship between fibrosis and diastolic function using correlations and found a significant correlation between fibrosis and diastolic function in vivo, as measured by chamber compliance (Fig. 3*E*).

PAB rats exhibited mitochondrial structural remodeling associated with increased oxygen consumption and decreased mechanical efficiency. Given that alterations in mitochondrial ultrastructure, including number and size, have been reported in heart failure (9, 15, 38), we examined changes in RV mitochondrial structure (Fig. 4, *A* and *B*). Mitochondria per HPF increased in PAB compared with sham rats (Fig. 4*C*), and the average size of the mitochondria was smaller in PAB rats (Fig. 4*D*). The total mitochondrial mass in the RV free wall, as determined from measured mitochondrial volume fraction and RV weight, also increased with PAB (Fig. 4*E*).

We explored potential mechanisms of altered mitochondrial ultrastructure by quantifying the gene expression of PGC-1α, a master regulator of mitochondrial biogenesis (24, 37) and an important regulator of oxidative metabolism (12). PGC-1α expression was significantly decreased in the PAB group compared with the sham group (Fig. 5).

To explore the impact of mitochondrial ultrastructural remodeling on RV organ level function, we examined oxygen consumption (as measured by PVA), EW, and mechanical efficiency. There was a nearly threefold increase in RV energy consumption in the PAB group (Fig. 6*A*). However, this was not translated into a proportional increase in external work (Fig. 6*B*) or, consequently, mechanical efficiency in the PAB group (Fig. 6*C*). We explored further potential mitochondrial structure-ventricular function relationships in RVF via statistical correlations. Mitochondrial mass showed a strong direct correlation with oxygen consumption (Fig. 7*A*) and an inverse correlation with mechanical efficiency (Fig. 7*D*). Mitochondrial mass also correlated well with other organ-level parameters such as RV mass ($r^2 = 0.97$, $P < 0.005$) and contractility dP/dt_{max} ($r^2 = 0.61$, $P < 0.05$) (data not shown). Similar to mitochondrial mass, mitochondria per HPF had a direct correlation with oxygen consumption (Fig. 7*B*) and an inverse correlation to mechanical efficiency, which did not reach statistical significance (Fig. 7*E*). The correlation between reduced mitochondrial size and reduced mechanical efficiency also did not reach statistical significance (Fig. 7*F*). Taken together, these significant relationships suggest that mitochondrial mass and number are increased in RVF due to increased energy demands in the setting of pressure overload. Translation of this energy into external work is somewhat impaired by mitochondrial structural changes, but mitochondrial functional

Table 2. *Body weight and morphological parameters of the RV and LV*

	Sham	PAB
Body weight, g	468.6 ± 60.0	454.5 ± 26.2
RV, mg	195.8 ± 10.5	485.0 ± 130.0*
LV + septum, mg	822.8 ± 77.2	819.5 ± 56.9
RV/body weight, mg/g	0.42 ± 0.04	1.06 ± 0.25*
RV/LV + septum, mg/mg	0.24 ± 0.02	0.60 ± 0.19*

Values are means ± SD; $n = 8$ sham and 10 pulmonary artery banded (PAB) rats. RV, right ventricle; LV, left ventricle plus septum weight. Body weight, RV free wall weight, and LV + septum weight were measured in PAB and sham rats at the terminal time point to calculate RV hypertrophy, as represented by RV weight relative to body weight and RV weight relative to the LV + septum. Significant differences compared with sham rats using a two-tailed Student's *t*-test are shown as *$P < 0.005$, sham vs. PAB.

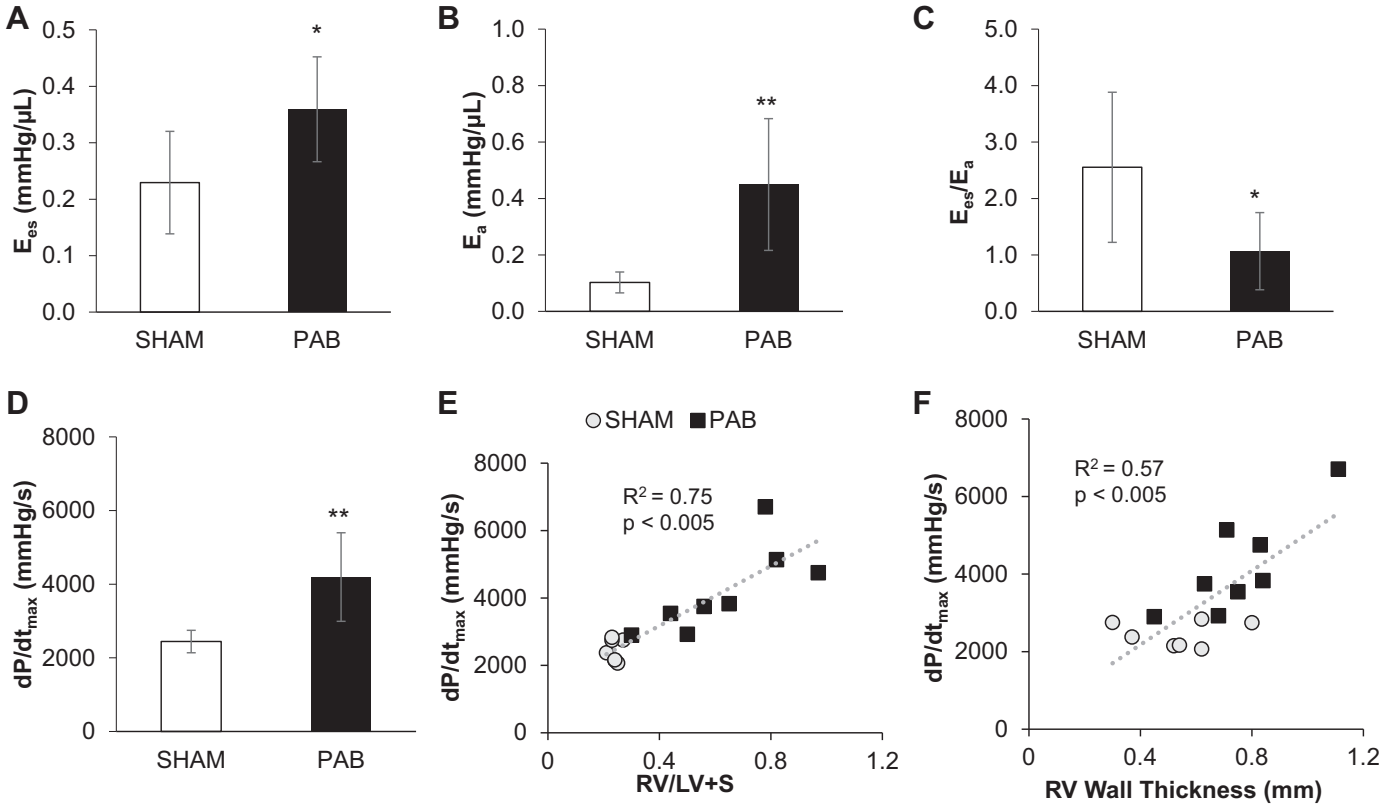

Fig. 2. *A–C*: pulmonary artery banded (PAB) rats displayed increased end-systolic elastance (E_{es}; *A*), elevated arterial elastance (E_a; *B*), and decreased ventricular-vascular coupling (E_{es}/E_a; *C*) compared with sham rats. *D–F*: PAB resulted in an elevated maximal derivative of pressure (dP/dt_{max}) compared with the sham group (*D*), which was positively correlated to right ventricular (RV) weight relative to left ventricular and septum weights (LV + S; *E*) and echocardiography-derived RV wall thickness (*F*). Pearson's correlation indicated the statistically significant relationships between RV hypertrophy and contractility. In *A–D*, data are presented as means ± SD. In *E* and *F*, data are presented as measurements taken from each PAB and sham rat; $n = 7$ sham and 8 PAB rats. A two-tailed Student's *t*-test was used to determine significant differences between groups. *$P < 0.05$ and **$P < 0.005$, sham vs. PAB.

changes, not measured here, likely contribute to mechanical inefficiency.

DISCUSSION

This study demonstrates structure-function relationships across multiple scales in RVF. At the organ level, hypertrophic remodeling and increased contractility in response to pressure overload were strongly correlated, as expected. A direct tissue-organ link between ventricular fibrosis and diastolic dysfunction was found, in confirmation of prior in vitro work. Also, for the first time, ultrastructural changes in mitochondria and increased mitochondrial mass were found to associate with hemodynamic estimates of RV oxygen consumption, which constitutes an organelle-organ link.

Table 3. *Hemodynamic parameters measured using right heart catheterization in vivo*

	Sham	PAB
Systolic pressure, mmHg	110 ± 14	122 ± 23
End-diastolic pressure, mmHg	4.5 ± 1.9	6.5 ± 2.0
End-diastolic volume, μl	447 ± 88	473 ± 68
Cardiac index, ml·min^{-1}·kg^{-1}	264 ± 74	149 ± 74*
dP/dt_{min}, mmHg/s	−1,816 ± 335	−2,705 ± 692*
dP/dt_{max}-V_{ed}, mmHg·μl^{-1}·s^{-1}	6.07 ± 1.68	9.89 ± 1.96*

Values are means ± SD; $n = 7$ sham and 8 pulmonary artery banded (PAB) rats. dP/dt_{min} minimal derivative of pressure; dP/dt_{max}, maximal derivative of pressure. Systolic pressure, end-diastolic pressure, end-diastolic volume, cardiac output relative to body weight (cardiac index), and relation of dP/dt_{max} to end-diastolic volume were determined for sham and PAB rats. A two-tailed Student's *t*-test was used to show significant difference between both groups. *$P < 0.05$, sham vs. PAB.

Hypertrophic remodeling is a well-established response of the RV to pressure overload, and the accepted paradigm is that RVF occurs when adaptive remodeling, including RV hypertrophy, is insufficient to compensate for the persistent RV afterload (7, 8, 49). Bogaard et al. (2) demonstrated RV hypertrophy occurring in response to PAH in both PAB without RVF and sugen-hypoxia-induced RVF. Our laboratory has shown early development of RV hypertrophy that plateaued after 3 wk of sugen-hypoxia exposure, with a similar pattern of increase in E_{es} in the same model (52). The present work is consistent with these previous findings and additionally demonstrates a strong, direct correlation between RV hypertrophy and contractility on an individual animal basis. Despite these adaptive changes, RVF is present at 8 wk postbanding, as evidenced by decreased EF, decreased CO, and ventricular-vascular uncoupling.

RV fibrosis consistently develops in response to pressure overload and is a hallmark of RVF (2, 11, 34, 35). Previous work from our laboratory showed progressive fibrosis associated with progressive diastolic dysfunction, as measured by chamber compliance in sugen-hypoxia-induced RV dys-

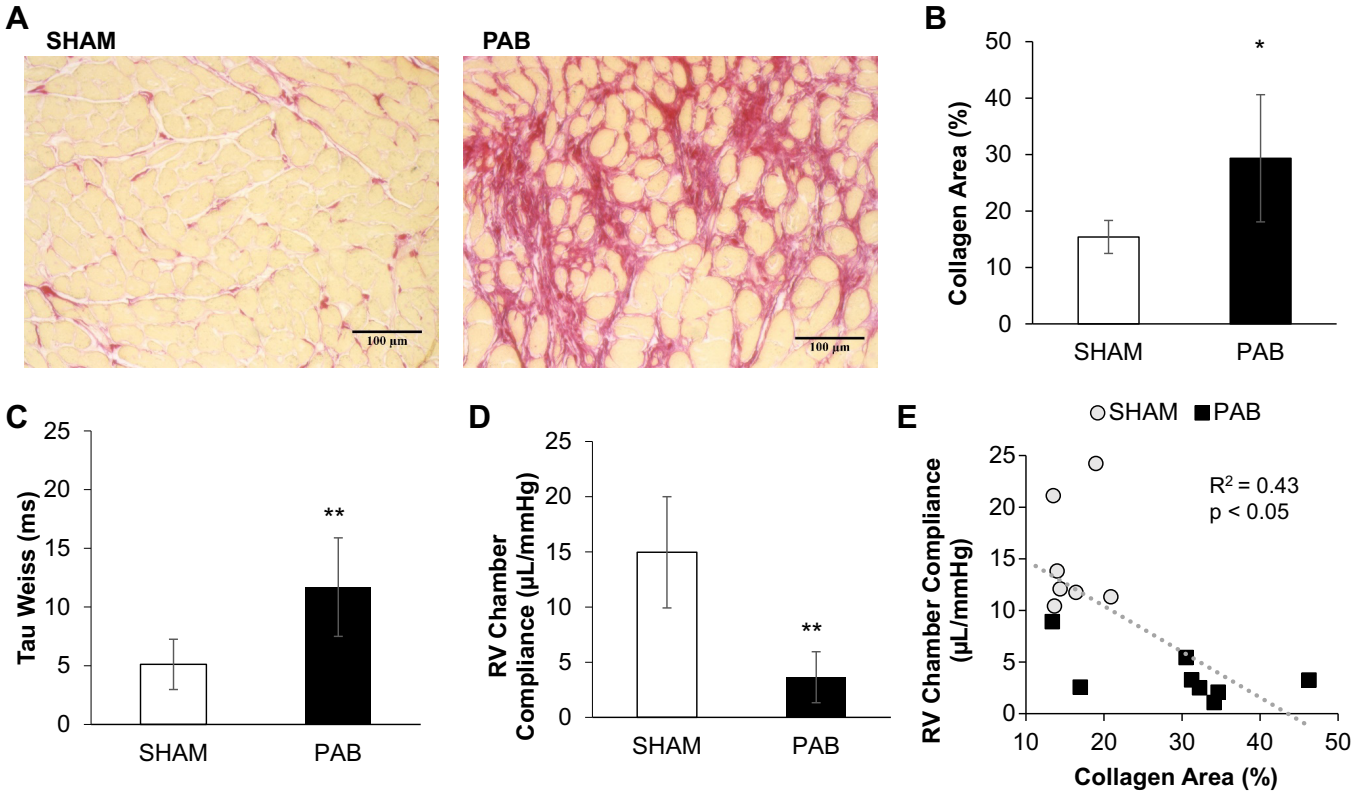

Fig. 3. *A*: representative images of right ventricular (RV) tissue stained with picrosirius red demonstrating collagen accumulation in pulmonary artery banded (PAB) rats. *B–D*: PAB rats displayed a significant increase in collagen deposition (*B*), an increase in the isovolumic relaxation time constant (τ Weiss; *C*), and a decrease in RV chamber compliance (*D*) compared with sham rats. *E*: collagen deposition in the RV was positively correlated to RV chamber compliance. Pearson's correlation indicated the statistically significant relationship between collagen deposition and RV stiffness. In *B–D*, data are presented as means ± SD. In *E*, data are presented as measurements taken from each PAB and sham rat; $n = 7–8$ sham and 8–10 PAB rats. A two-tailed Student's *t*-test was used to determine significant differences between groups. $^*P < 0.05$ and $^{**}P < 0.005$, sham vs. PAB.

function (52). Recent work by Rain et al. (34) has focused on the contribution of collagen accumulation to myocardial stiffness measured in skinned trabeculea after PAB in rats. The present study builds on the in vitro findings of Rain et al. (34), showing a direct correlation between myocardial collagen content and myocardial stiffness measured in vivo as chamber compliance on an individual animal basis. In addition to impaired chamber compliance, which reflects slowed passive relaxation, prolonged τ Weiss, which reflects slowed active relaxation, was observed in our study. Beyond collagen accumulation, tissue level myocardial stiffness can also be due to intrinsic cardiomyocyte stiffening, which likely accounts for the increase in τ Weiss. Indeed, Rain et al. (34) demonstrated that changes in phosphorylation levels of titin isoform are associated with cardiomyocyte stiffening in PAB rats, suggesting that titin hypophosphorylation accounts for this intrinsic change in cardiomyoctes. Recent studies by our group and others have demonstrated increased passive tension in isolated RV cardiomyocytes in rodent models of PAH (30, 51), suggesting intrinsic changes in the cardiomyocytes contributing to the inability of the muscle fibers to return to normal lengths.

Mitochondria are the cellular powerhouses responsible for energy production necessary to sustain cardiac contraction and relaxation (36). Abnormalities in mitochondrial structure, specifically reduced mitochondrial cross-sectional area and increased number, have been found in LV failure (9, 38). These changes in mitochondrial ultrastructure were associated with increased mitochondrial injury (38) and impaired mitochondrial fusion (9). Gomez-Arroyo et al. (15) examined mitochondria in the setting of RVF and demonstrated impaired mitochondrial respiration, which was associated with abnormal mitochondrial ultrastructure. There is a clear, well-established link between mitochondrial ultrastructure and function (19, 20); however, the impact of these observed mitochondrial changes on RV hemodynamic function, particularly mechanical efficiency, has not been explored.

To our knowledge, this is the first study to demonstrate RV mechanical inefficiency in RVF. Using measurement and analysis methods similar to ours, increased RV oxygen consumption and mechanical inefficiency have previously been shown in sugen-hypoxia-exposed rats that developed RV dysfunction (25). Importantly, this study also evaluated mitochondrial content and found increased RV mitochondrial amount, as measured by citrate synthase activity, but reduced mitochondrial density (25). The present study is consistent with previous reports in both RV and LV, showing increased total mitochondrial mass in the RV and increased mitochondrial number as well as reduced mitochondrial size. More importantly, the current work goes beyond previous reports to show a direct correlation between changes in mitochondrial mass and number and increase in oxygen consumption. This increase in consumption is not translated into a proportional increase in external work, resulting in mechanical inefficiency. It is likely

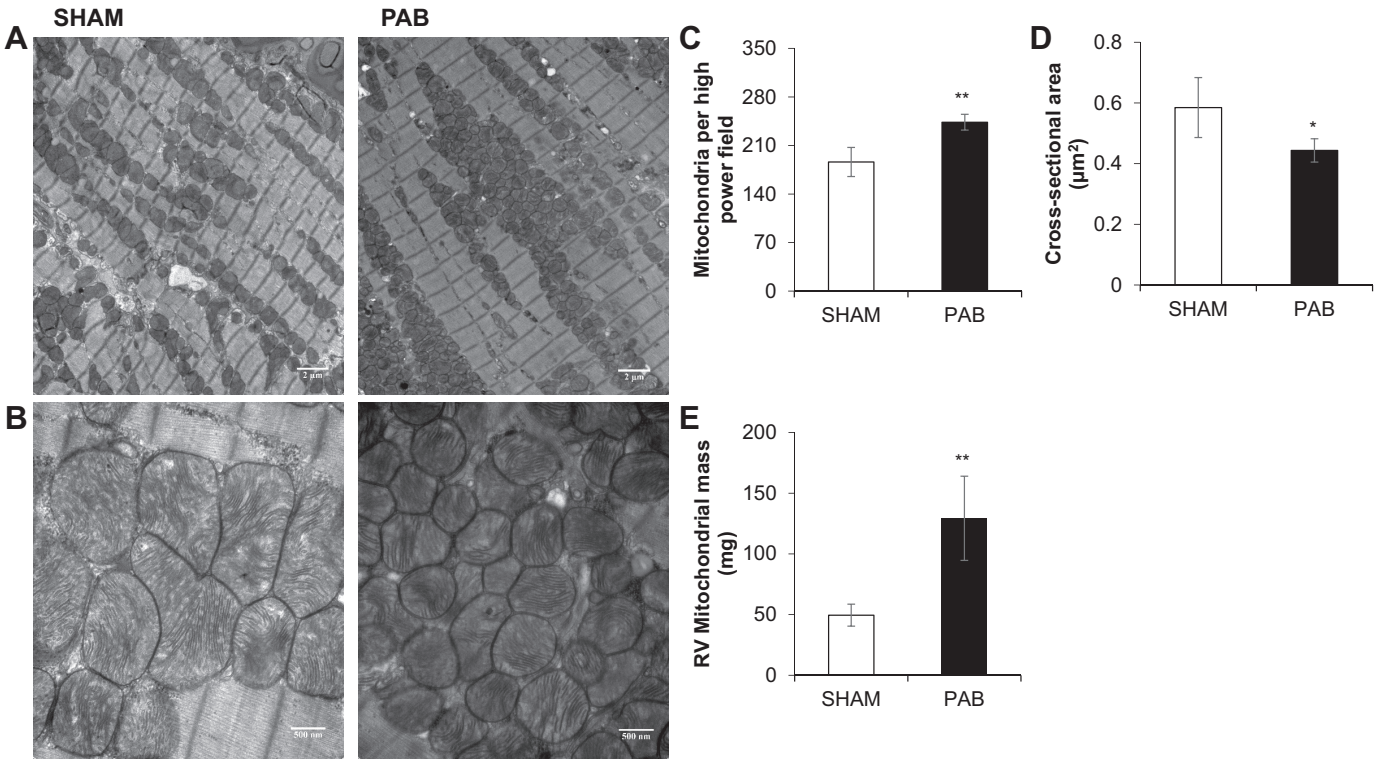

Fig. 4. *A* and *B*: representative electron micrographs of mitochondria from the right ventricle (RV) of sham and pulmonary artery banded (PAB) rats taken at ×5,600 (*A*) and ×25,000 (*B*) magnifications. *C–E*: PAB rats exhibited increased number of mitochondria per high-power field (*C*), decreased cross-sectional area (*D*), and increased RV mitochondrial mass (*E*) compared with sham rats. Data are presented as means ± SD; $n = 5$ for both sham and PAB rats. A two-tailed Student's *t*-test was used to determine significant differences between groups. $^*P < 0.05$ and $^{**}P < 0.005$, sham vs. PAB.

that although the total number and mass of mitochondria increase as RV mass increases in response to pressure overload, mitochondria become structurally and functionally impaired, as suggested by reduced size and downregulation of PGC-1α.

Downregulation of PGC-1α is a consistent feature associated with mitochondrial abnormalities in the failing RV (15) and LV (6, 13). Our finding of decreased PGC-1α expression is consistent with previous work that has demonstrated a trend toward decreased PGC-1α gene expression in patients with RVF and in rats with sugen-hypoxia-induced PAH (15, 25). In a rat model of sugen-hypoxia-induced RVF, Gomez-Arroyo et al. (15) demonstrated that changes in PGC-1α gene expression were associated with impaired mitochondrial respiratory capacity as well as abnormal mitochondrial ultrastructure. They further showed that decreases in PGC-1α expression were associated with decreases in estrogen-related receptor-α and PPAR-α, two downstream effectors of PGC-1α that are critical regulators of fatty acid oxidation (15). Downregulation of PGC-1α has also been demonstrated in LV failure and as in this study associated with mitochondrial ultrastructural abnormalities (6, 13). The mechanisms driving reduced PGC-1α in RVF and the impact of PGC-1α on mitochondrial ultrastructure and function are still being investigated.

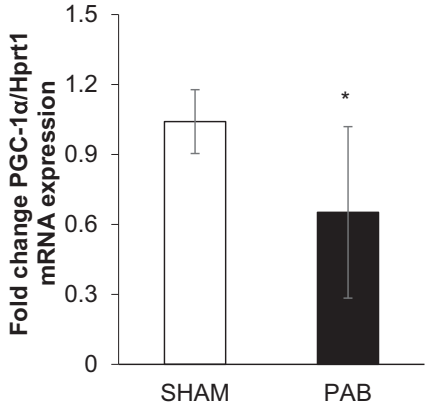

Fig. 5. Peroxisome proliferator-activated receptor-γ coactivator-1α (PGC-1α) is downregulated in the right ventricle of pulmonary artery banded (PAB) rats compared with sham rats. Hypoxanthine phosphoribosyltransferase 1 (Hprt1) was used as the housekeeping gene. Data are presented as means ± SD; $n = 8$ sham and 10 PAB rats. A two-tailed Student's *t*-test was used to determine significant differences between groups. $^*P < 0.05$, sham vs. PAB.

Although this study provides key evidence of structure-function relationships in RVF, there are several limitations that should be noted. Only one time point postbanding was evaluated invasively. Thus, associations can be determined, but causal relationships and the relative timing of structural remodeling and functional impairments cannot be determined. Additionally, analysis of structure-function relationships focused on correlations between individual structural and functional changes. Clearly, multiple mechanical and biochemical factors contribute to each aspect of organ level function, and many of these factors are not accounted for in this analysis. Similarly, it is likely that each structural change impacts multiple facets of organ level function. For example, mitochondrial function may impact contractility via alterations in metabolite levels or

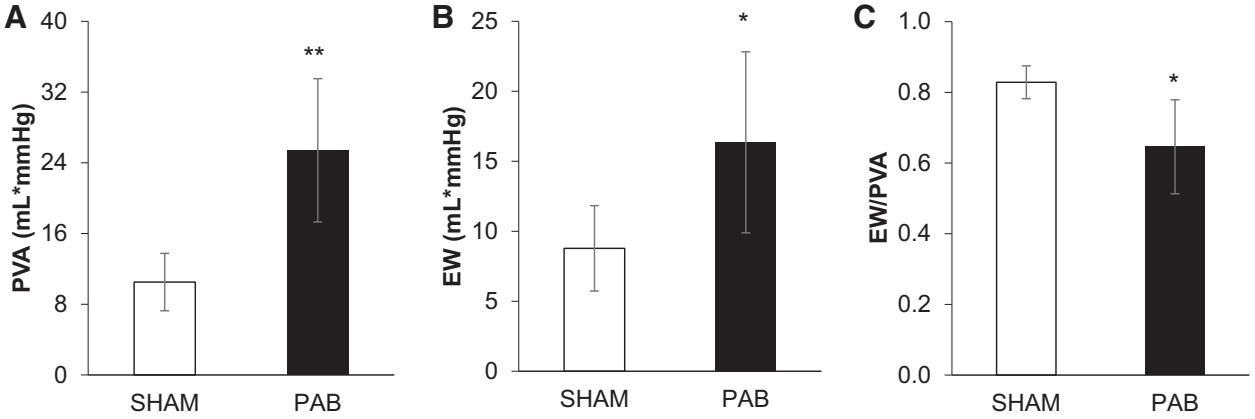

Fig. 6. Pulmonary artery banded (PAB) rats demonstrated an elevated pressure-volume area (PVA; *A*), increased external work (EW; *B*), and reduced mechanical efficiency (EW/PVA; *C*) compared with sham rats. Data are presented as means ± SD; $n = 7$ sham and 8 PAB rats. A two-tailed Student's *t*-test was used to determine significant differences between groups. $^*P < 0.05$ and $^{**}P < 0.005$, sham vs. PAB.

contribute to fibrosis and diastolic dysfunction through production of reactive oxygen species. Additionally, neither mitochondrial function nor mitochondrial enzyme activity was assessed. Although there is a demonstrated link between mitochondrial utlrastructure and function (19, 20), conclusions about the impact of mitochondrial changes observed in RVF are limited by the lack of functional measurements to accompany ultrastructural measurements. Further exploration of structure-function relationships in the RV to further delineate the interactions is an important area of future research that will hopefully provide insight into disease mechanisms and help guide development of effective therapies.

The determintation of PVA from pressure-volume loops has been shown to be closely correlated to myocardial oxygen consumption (46). This methodology has been used by many researchers to examine energy consumption, output, and, therefore, efficiency from invasive hemodynamics in both the LV and RV (14, 21, 25, 26, 32, 43, 44). However, it is not a direct measurement of oxygen consumption, and it is essential to note this as a key limitation in the current study. Future studies should include direct measurements of both ventricular and mitochondrial oxygen consumption as well as metabolite production to better assess and understand their interdependent relationship.

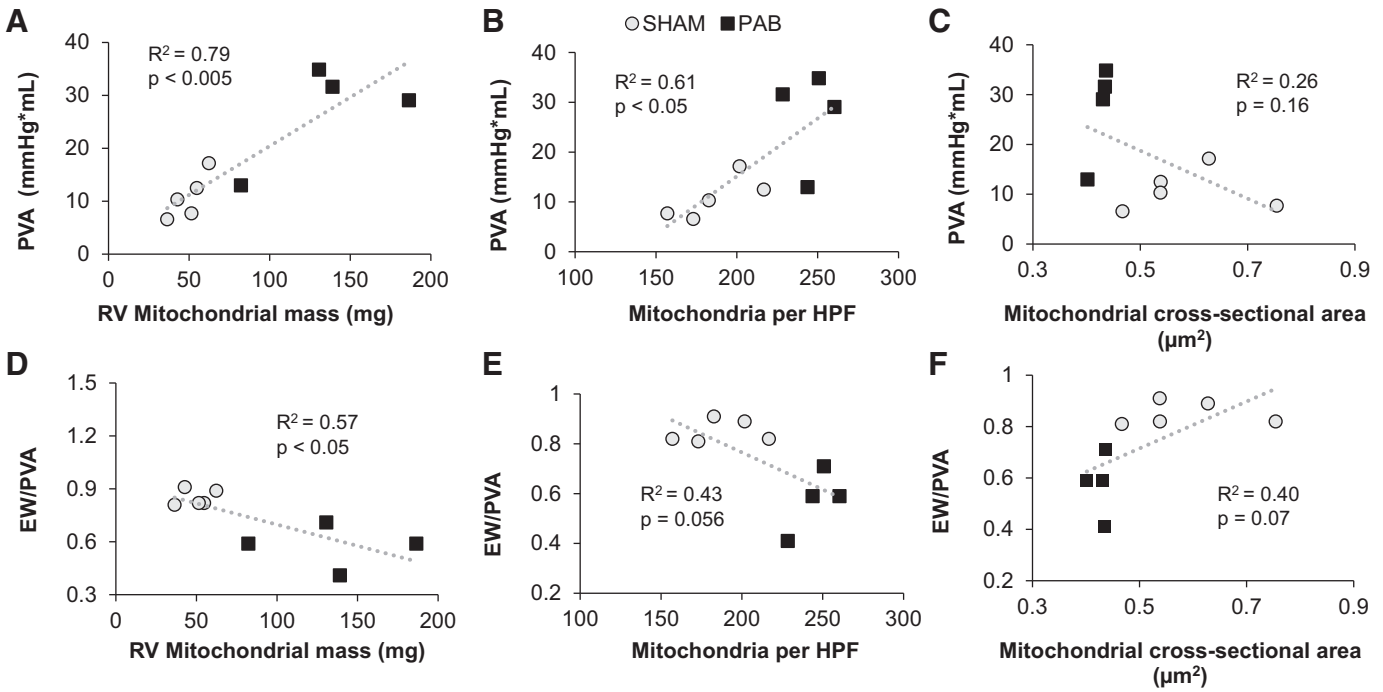

Fig. 7. *A–C*: pressure-volume area (PVA) was correlated to right ventricular (RV) mitochondrial mass (*A*), number of mitochondria per high-power field (HPF; *B*), and mitochondrial cross-sectional area (*C*) in pulmonary artery banded (PAB) and sham rats. *D–F*: mechanical efficiency (EW/PVA) showed correlations with mitochondrial mass (*D*), number of mitochondria (*E*), and mitochondrial cross-sectional area (*F*). Pearson's correlation indicated the statistically significant relationship between mitochondrial changes and RV mechanoenergetics. Data are presented as measurements taken from each PAB and sham rat; $n = 5$ sham and 4 PAB rats.

Conclusions

In summary, this work provides important insights into the functional impact of multiscale ventricular remodeling. It provides strong evidence to support the established understanding of the adaptive, protective impact of hypertrophy on increasing contractility. The study gives strong in vivo evidence to support recent in vitro work demonstrating the contribution of collagen deposition to impaired diastolic function. In the setting of an ever-growing focus on metabolic remodeling in RVF, this work is among the first to quantify mitochondrial ultrastructural remodeling in RVF as well as demonstrate mechanical inefficiency as a hemodynamic feature of RVF. Going further, this study demonstrates a correlation between increasing mitochondrial amount and oxygen consumption in RVF.

ACKNOWLEDGMENTS

We thank Gaoussou Diara, Allison Brodbeck, Randy Massey, and Bilin Loi for technical expertise and valuable help with the surgery, echocardiography, electron microscopy, and caretaking of the animals. We are grateful to Dr. Mark Golob, David Schreier, Ryan Pewowaruk, and Dr. Juan Sebastian Danobeitia for helpful discussions.

GRANTS

This work was supported in part by a Thoracic Surgery Foundation Nina Starr Braunwald Research Fellowship (to J. L. Philip) and National Heart, Lung, and Blood Institute Grants R01-HL-086939 (to N. C. Chesler), T32-HL-007936 (to T. -C. Cheng), and T32-HL-110853 (to J. L. Philip).

DISCLOSURES

No conflicts of interest, financial or otherwise, are declared by the authors.

AUTHOR CONTRIBUTIONS

T.-C.C., D.M.T., and N.C.C. conceived and designed research; T.-C.C., D.M.T., and T.A.H. performed experiments; T.-C.C., J.L.P., and D.M.T. analyzed data; T.-C.C., J.L.P., D.M.T., T.A.H., and N.C.C. interpreted results of experiments; T.-C.C., J.L.P., and D.M.T. prepared figures; T.-C.C., J.L.P., D.M.T., and N.C.C. drafted manuscript; T.-C.C., J.L.P., D.M.T., T.A.H., and N.C.C. edited and revised manuscript; T.-C.C., J.L.P., D.M.T., T.A.H., and N.C.C. approved final version of manuscript.

REFERENCES

1. **Benjamin EJ, Blaha MJ, Chiuve SE, Cushman M, Das SR, Deo R, de Ferranti SD, Floyd J, Fornage M, Gillespie C, Isasi CR, Jiménez MC, Jordan LC, Judd SE, Lackland D, Lichtman JH, Lisabeth L, Liu S, Longenecker CT, Mackey RH, Matsushita K, Mozaffarian D, Mussolino ME, Nasir K, Neumar RW, Palaniappan L, Pandey DK, Thiagarajan RR, Reeves MJ, Ritchey M, Rodriguez CJ, Roth GA, Rosamond WD, Sasson C, Towfighi A, Tsao CW, Turner MB, Virani SS, Voeks JH, Willey JZ, Wilkins JT, Wu JH, Alger HM, Wong SS, Muntner P; American Heart Association Statistics Committee and Stroke Statistics Subcommittee.** Heart Disease and Stroke Statistics-2017 Update: a report from the American Heart Association. *Circulation* 135: e146–e603, 2017. [Erratum in *Circulation* 135: e646, 2017. 10.1161/CIR.0000000000000491 28264899.] doi:10.1161/CIR.0000000000000485.
2. **Bogaard HJ, Natarajan R, Henderson SC, Long CS, Kraskauskas D, Smithson L, Ockaili R, McCord JM, Voelkel NF.** Chronic pulmonary artery pressure elevation is insufficient to explain right heart failure. *Circulation* 120: 1951–1960, 2009. doi:10.1161/CIRCULATIONAHA.109.883843.
3. **Borgdorff MA, Bartelds B, Dickinson MG, Steendijk P, Berger RM.** A cornerstone of heart failure treatment is not effective in experimental right ventricular failure. *Int J Cardiol* 169: 183–189, 2013. doi:10.1016/j.ijcard.2013.08.102.
4. **Borgdorff MA, Koop AM, Bloks VW, Dickinson MG, Steendijk P, Sillje HH, van Wiechen MP, Berger RM, Bartelds B.** Clinical symptoms of right ventricular failure in experimental chronic pressure load are associated with progressive diastolic dysfunction. *J Mol Cell Cardiol* 79: 244–253, 2015. doi:10.1016/j.yjmcc.2014.11.024.
5. **Brown DA, Perry JB, Allen ME, Sabbah HN, Stauffer BL, Shaikh SR, Cleland JG, Colucci WS, Butler J, Voors AA, Anker SD, Pitt B, Pieske B, Filippatos G, Greene SJ, Gheorghiade M.** Expert consensus document: mitochondrial function as a therapeutic target in heart failure. *Nat Rev Cardiol* 14: 238–250, 2017. doi:10.1038/nrcardio.2016.203.
6. **Bugger H, Schwarzer M, Chen D, Schrepper A, Amorim PA, Schoepe M, Nguyen TD, Mohr FW, Khalimonchuk O, Weimer BC, Doenst T.** Proteomic remodelling of mitochondrial oxidative pathways in pressure overload-induced heart failure. *Cardiovasc Res* 85: 376–384, 2010. doi:10.1093/cvr/cvp344.
7. **Champion HC, Michelakis ED, Hassoun PM.** Comprehensive invasive and noninvasive approach to the right ventricle-pulmonary circulation unit: state of the art and clinical and research implications. *Circulation* 120: 992–1007, 2009. doi:10.1161/CIRCULATIONAHA.106.674028.
8. **Chemla D, Castelain V, Hervé P, Lecarpentier Y, Brimioulle S.** Haemodynamic evaluation of pulmonary hypertension. *Eur Respir J* 20: 1314–1331, 2002. doi:10.1183/09031936.02.00068002.
9. **Chen L, Gong Q, Stice JP, Knowlton AA.** Mitochondrial OPA1, apoptosis, and heart failure. *Cardiovasc Res* 84: 91–99, 2009. doi:10.1093/cvr/cvp181.
10. **D'Alonzo GE, Barst RJ, Ayres SM, Bergofsky EH, Brundage BH, Detre KM, Fishman AP, Goldring RM, Groves BM, Kernis JT, Levy PS, Petra GG, Reid LM, Reeves JT, Rich S, Vreim CE, Williams GW, Wu M.** Survival in patients with primary pulmonary hypertension. Results from a national prospective registry. *Ann Intern Med* 115: 343–349, 1991. doi:10.7326/0003-4819-115-5-343.
11. **Drake JI, Bogaard HJ, Mizuno S, Clifton B, Xie B, Gao Y, Dumur CI, Fawcett P, Voelkel NF, Natarajan R.** Molecular signature of a right heart failure program in chronic severe pulmonary hypertension. *Am J Respir Cell Mol Biol* 45: 1239–1247, 2011. doi:10.1165/rcmb.2010-0412OC.
12. **Finck BN, Kelly DP.** Peroxisome proliferator-activated receptor gamma coactivator-1 (PGC-1) regulatory cascade in cardiac physiology and disease. *Circulation* 115: 2540–2548, 2007. doi:10.1161/CIRCULATIONAHA.107.670588.
13. **Garnier A, Fortin D, Deloménie C, Momken I, Veksler V, Ventura-Clapier R.** Depressed mitochondrial transcription factors and oxidative capacity in rat failing cardiac and skeletal muscles. *J Physiol* 551: 491–501, 2003. doi:10.1113/jphysiol.2003.045104.
14. **Golob MJ, Wang Z, Prostrollo AJ, Hacker TA, Chesler NC.** Limiting collagen turnover via collagenase-resistance attenuates right ventricular dysfunction and fibrosis in pulmonary arterial hypertension. *Physiol Rep* 4: e12815, 2016. doi:10.14814/phy2.12815.
15. **Gomez-Arroyo J, Mizuno S, Szczepanek K, Van Tassell B, Natarajan R, dos Remedios CG, Drake JI, Farkas L, Kraskauskas D, Wijesinghe DS, Chalfant CE, Bigbee J, Abbate A, Lesnefsky EJ, Bogaard HJ, Voelkel NF.** Metabolic gene remodeling and mitochondrial dysfunction in failing right ventricular hypertrophy secondary to pulmonary arterial hypertension. *Circ Heart Fail* 6: 136–144, 2013. doi:10.1161/CIRCHEARTFAILURE.111.966127.
16. **Goss KN, Cucci AR, Fisher AJ, Albrecht M, Frump A, Tursunova R, Gao Y, Brown MB, Petrache I, Tepper RS, Ahlfeld SK, Lahm T.** Neonatal hyperoxic lung injury favorably alters adult right ventricular remodeling response to chronic hypoxia exposure. *Am J Physiol Lung Cell Mol Physiol* 308: L797–L806, 2015. doi:10.1152/ajplung.00276.2014.
17. **Greyson CR.** Pathophysiology of right ventricular failure. *Crit Care Med* 36, *Suppl*: S57–S65, 2008. doi:10.1097/01.CCM.0000296265.52518.70.
18. **Hoeper MM, Humbert M, Souza R, Idrees M, Kawut SM, Sliwa-Hahnle K, Jing Z-C, Gibbs JSR.** A global view of pulmonary hypertension. *Lancet Respir Med* 4: 306–322, 2016. doi:10.1016/S2213-2600(15)00543-3.
19. **Hollander JM, Thapa D, Shepherd DL.** Physiological and structural differences in spatially distinct subpopulations of cardiac mitochondria: influence of cardiac pathologies. *Am J Physiol Heart Circ Physiol* 307: H1–H14, 2014. doi:10.1152/ajpheart.00747.2013.
20. **Hoppel CL, Tandler B, Fujioka H, Riva A.** Dynamic organization of mitochondria in human heart and in myocardial disease. *Int J Biochem Cell Biol* 41: 1949–1956, 2009. doi:10.1016/j.biocel.2009.05.004.
21. **Johnson RC, Datar SA, Oishi PE, Bennett S, Maki J, Sun C, Johengen M, He Y, Raff GW, Redington AN, Fineman JR.** Adaptive right ventricular performance in response to acutely increased afterload in a

lamb model of congenital heart disease: evidence for enhanced Anrep effect. *Am J Physiol Heart Circ Physiol* 306: H1222–H1230, 2014. doi:10.1152/ajpheart.01018.2013.

22. **Joshi DC, Zhang CL, Lin TM, Gusain A, Harris MG, Tree E, Yin Y, Wu C, Sheng ZH, Dempsey RJ, Fabry Z, Chiu SY.** Deletion of mitochondrial anchoring protects dysmyelinating shiverer: implications for progressive MS. *J Neurosci* 35: 5293–5306, 2015. doi:10.1523/JNEUROSCI.3859-14.2015.
23. **Kelly RP, Ting CT, Yang TM, Liu CP, Maughan WL, Chang MS, Kass DA.** Effective arterial elastance as index of arterial vascular load in humans. *Circulation* 86: 513–521, 1992. doi:10.1161/01.CIR.86.2.513.
24. **Lehman JJ, Barger PM, Kovacs A, Saffitz JE, Medeiros DM, Kelly DP.** Peroxisome proliferator-activated receptor gamma coactivator-1 promotes cardiac mitochondrial biogenesis. *J Clin Invest* 106: 847–856, 2000. doi:10.1172/JCI10268.
25. **Liu A, Philip J, Vinnakota KC, Van den Bergh F, Tabima DM, Hacker T, Beard DA, Chesler NC.** Estrogen maintains mitochondrial content and function in the right ventricle of rats with pulmonary hypertension. *Physiol Rep* 5: e13157, 2017. doi:10.14814/phy2.13157.
26. **Liu A, Schreier D, Tian L, Eickhoff JC, Wang Z, Hacker TA, Chesler NC.** Direct and indirect protection of right ventricular function by estrogen in an experimental model of pulmonary arterial hypertension. *Am J Physiol Heart Circ Physiol* 307: H273–H283, 2014. doi:10.1152/ajpheart.00758.2013.
28. **Livak KJ, Schmittgen TD.** Analysis of relative gene expression data using real-time quantitative PCR and the 2(−Delta Delta C(T)) method. *Methods* 25: 402–408, 2001. doi:10.1006/meth.2001.1262.
29. **Markel TA, Wairiuko GM, Lahm T, Crisostomo PR, Wang M, Herring CM, Meldrum DR.** The right heart and its distinct mechanisms of development, function, and failure. *J Surg Res* 146: 304–313, 2008. doi:10.1016/j.jss.2007.04.003.
30. **Mendes-Ferreira P, Santos-Ribeiro D, Adão R, Maia-Rocha C, Mendes-Ferreira M, Sousa-Mendes C, Leite-Moreira AF, Brás-Silva C.** Distinct right ventricle remodeling in response to pressure overload in the rat. *Am J Physiol Heart Circ Physiol* 311: H85–H95, 2016. doi:10.1152/ajpheart.00089.2016.
31. **Nouette-Gaulain K, Malgat M, Rocher C, Savineau JP, Marthan R, Mazat JP, Sztark F.** Time course of differential mitochondrial energy metabolism adaptation to chronic hypoxia in right and left ventricles. *Cardiovasc Res* 66: 132–140, 2005. doi:10.1016/j.cardiores.2004.12.023.
32. **Nozawa T, Yasumura Y, Futaki S, Tanaka N, Uenishi M, Suga H.** Efficiency of energy transfer from pressure-volume area to external mechanical work increases with contractile state and decreases with afterload in the left ventricle of the anesthetized closed-chest dog. *Circulation* 77: 1116–1124, 1988. doi:10.1161/01.CIR.77.5.1116.
33. **Picard M, White K, Turnbull DM.** Mitochondrial morphology, topology, and membrane interactions in skeletal muscle: a quantitative three-dimensional electron microscopy study. *J Appl Physiol* 114: 161–171, 2013. doi:10.1152/japplphysiol.01096.2012.
34. **Rain S, Andersen S, Najafi A, Gammelgaard Schultz J, da Silva Gonçalves Bós D, Handoko ML, Bogaard HJ, Vonk-Noordegraaf A, Andersen A, van der Velden J, Ottenheijm CA, de Man FS.** Right ventricular myocardial stiffness in experimental pulmonary arterial hypertension: relative contribution of fibrosis and myofibril stiffness. *Circ Heart Fail* 9: e002636, 2016. doi:10.1161/CIRCHEARTFAILURE.115.002636.
35. **Rain S, Handoko ML, Trip P, Gan CT, Westerhof N, Stienen GJ, Paulus WJ, Ottenheijm CA, Marcus JT, Dorfmüller P, Guignabert C, Humbert M, Macdonald P, Dos Remedios C, Postmus PE, Saripalli C, Hidalgo CG, Granzier HL, Vonk-Noordegraaf A, van der Velden J, de Man FS.** Right ventricular diastolic impairment in patients with pulmonary arterial hypertension. *Circulation* 128: 2016–2025, 2013. doi:10.1161/CIRCULATIONAHA.113.001873.
36. **Rosca MG, Tandler B, Hoppel CL.** Mitochondria in cardiac hypertrophy and heart failure. *J Mol Cell Cardiol* 55: 31–41, 2013. doi:10.1016/j.yjmcc.2012.09.002.
37. **Russell LK, Mansfield CM, Lehman JJ, Kovacs A, Courtois M, Saffitz JE, Medeiros DM, Valencik ML, McDonald JA, Kelly DP.** Cardiac-specific induction of the transcriptional coactivator peroxisome proliferator-activated receptor gamma coactivator-1alpha promotes mitochondrial biogenesis and reversible cardiomyopathy in a developmental stage-dependent manner. *Circ Res* 94: 525–533, 2004. doi:10.1161/01.RES.0000117088.36577.EB.
38. **Sabbah HNSV, Sharov V, Riddle JM, Kono T, Lesch M, Goldstein S.** Mitochondrial abnormalities in myocardium of dogs with chronic heart failure. *J Mol Cell Cardiol* 24: 1333–1347, 1992. doi:10.1016/0022-2828(92)93098-5.
39. **Sagawa K.** The end-systolic pressure-volume relation of the ventricle: definition, modifications and clinical use. *Circulation* 63: 1223–1227, 1981. doi:10.1161/01.CIR.63.6.1223.
40. **Schreier D, Hacker T, Song G, Chesler N.** The role of collagen synthesis in ventricular and vascular adaptation to hypoxic pulmonary hypertension. *J Biomech Eng* 135: 021018, 2013. doi:10.1115/1.4023480.
41. **Schreier DA, Hacker TA, Hunter K, Eickoff J, Liu A, Song G, Chesler N.** Impact of increased hematocrit on right ventricular afterload in response to chronic hypoxia. *J Appl Physiol* 117: 833–839, 2014. doi:10.1152/japplphysiol.00059.2014.
42. **Spruijt OA, de Man FS, Groepenhoff H, Oosterveer F, Westerhof N, Vonk-Noordegraaf A, Bogaard HJ.** The effects of exercise on right ventricular contractility and right ventricular-arterial coupling in pulmonary hypertension. *Am J Respir Crit Care Med* 191: 1050–1057, 2015. doi:10.1164/rccm.201412-2271OC.
43. **Suga H.** Total mechanical energy of a ventricle model and cardiac oxygen consumption. *Am J Physiol* 236: H498–H505, 1979.
44. **Suga H, Hayashi T, Suehiro S, Hisano R, Shirahata M, Ninomiya I.** Equal oxygen consumption rates of isovolumic and ejecting contractions with equal systolic pressure-volume areas in canine left ventricle. *Circ Res* 49: 1082–1091, 1981. doi:10.1161/01.RES.49.5.1082.
45. **Suga H, Sagawa K.** Instantaneous pressure-volume relationships and their ratio in the excised, supported canine left ventricle. *Circ Res* 35: 117–126, 1974. doi:10.1161/01.RES.35.1.117.
46. **Suga H, Yamada O, Goto Y, Igarashi Y.** Oxygen consumption and pressure-volume area of abnormal contractions in canine heart. *Am J Physiol Heart Circ Physiol* 246: H154–H160, 1984.
47. **Tabima DM, Hacker TA, Chesler NC.** Measuring right ventricular function in the normal and hypertensive mouse hearts using admittance-derived pressure-volume loops. *Am J Physiol Heart Circ Physiol* 299: H2069–H2075, 2010. doi:10.1152/ajpheart.00805.2010.
48. **Vonk Noordegraaf A, Westerhof BE, Westerhof N.** The relationship between the right ventricle and its load in pulmonary hypertension. *J Am Coll Cardiol* 69: 236–243, 2017. doi:10.1016/j.jacc.2016.10.047.
49. **Vonk-Noordegraaf A, Haddad F, Chin KM, Forfia PR, Kawut SM, Lumens J, Naeije R, Newman J, Oudiz RJ, Provencher S, Torbicki A, Voelkel NF, Hassoun PM.** Right heart adaptation to pulmonary arterial hypertension: physiology and pathobiology. *J Am Coll Cardiol* 62, *Suppl*: D22–D33, 2013. doi:10.1016/j.jacc.2013.10.027.
50. **Wang Z, Lakes RS, Golob M, Eickhoff JC, Chesler NC.** Changes in large pulmonary arterial viscoelasticity in chronic pulmonary hypertension. *PLoS One* 8: e78569, 2013. doi:10.1371/journal.pone.0078569.
51. **Wang Z, Patel JR, Schreier DA, Hacker TA, Moss RL, Chesler NC.** Organ-level right ventricular dysfunction with preserved Frank-Starling mechanism in a mouse model of pulmonary arterial hypertension. *J Appl Physiol* 124: 1244–1253, 2018. doi:10.1152/japplphysiol.00725.2017.
52. **Wang Z, Schreier DA, Hacker TA, Chesler NC.** Progressive right ventricular functional and structural changes in a mouse model of pulmonary arterial hypertension. *Physiol Rep* 1: e00184, 2013. doi:10.1002/phy2.184.